Biomaterials 53 (2015) 274–284

Contents lists available at ScienceDirect

Biomaterials

journal homepage: www.elsevier.com/locate/biomaterials

Multifunctional effects of honokiol as an anti-inflammatory and anti-cancer drug in human oral squamous cancer cells and xenograft

Jin Hyoung Cho [a, 1], Young-Joo Jeon [a, 1], Seon-Min Park [b], Jae-Cheon Shin [b], Tae-Hoon Lee [c], Seunggon Jung [d], Hongju Park [e], Joohyun Ryu [f], Hanyong Chen [f], Zigang Dong [f], Jung-Hyun Shim [g, **], Jung-Il Chae [a, *]

[a] Department of Oral Pharmacology, School of Dentistry and Institute of Dental Bioscience, BK21 Plus, Chonbuk National University, Jeonju 651-756, Republic of Korea
[b] Pohang Center for Evaluation of Biomaterials, Pohang, Gyeongbuk, Republic of Korea
[c] Department of Oral Biochemistry, Dental Science Research Institute and the BK21 Project, Medical Research Center for Biomineralization Disorders, School of Dentistry, Chonnam National University, Gwangju, Republic of Korea
[d] Department of Oral and Maxillofacial Surgery, Chonnam National University Hwasun Hospital, Gwangju, Republic of Korea
[e] Department of Oral and Maxillofacial Surgery, School of Dentistry, Chonnam National University, Gwangju, Republic of Korea
[f] The Hormel Institute, University of Minnesota, Austin, MN, USA
[g] Department of Pharmacy, College of Pharmacy, Mokpo National University, Muan-gun, Jeonnam 534-729, Republic of Korea

ARTICLE INFO

Article history:
Received 31 October 2014
Received in revised form
16 February 2015
Accepted 21 February 2015
Available online

Keywords:
Proteomics
Honokiol
Endoplasmic reticulum resident protein 44
Oral squamous cell carcinoma
Apoptosis
Xenograft

ABSTRACT

The aim of this study was to investigate anti-inflammatory and anti-cancer effects of honokiol (HK) in two oral squamous cancer cell carcinoma (OSCC) cell lines, HN22 and HSC4, through the regulation of inducible nitric oxide synthase (iNOS) and endoplasmic reticulum resident protein 44 (ERp44). Griess assay, zymography, and quantitative PCR were performed to study iNOS expression and subsequent nitric oxide (NO) production in OSCC cell lines. Liquid chromatography-tandem mass spectrometry (LC-MS/MS)-based proteomic analysis was used to elucidate the proteins associated with ER stress and cellular cytotoxic response induced by HK. Pull-down assay and molecular modeling were performed to better understand how HK interacts with ERp44. *In vitro* and *in vivo* experiments in which ERp44 expression was knocked down were performed to better understand the effects of ERp44 on a cellular level and anti-cancer effects of HK. Expression levels of iNOS and subsequent NO secretion were reduced in OSCC cell lines treated with HK. ERp44 was significantly decreased in OSCC cell lines by HK treatment. HK directly bound to ERp44, and ERp44 knock-down significantly inhibited oral cancer cell proliferation and colony formation. Moreover, HK treatment effectively inhibited tumor growth and ERp44 levels in BALB/c nude mice bearing HN22 cell xenografts. Our findings suggest that HK inhibited inflammation and induced apoptosis by suppressing both iNOS/NO and ERp44 expression in HN22 and HSC4 cells and xenograft tumors, and thus could be a potent anti-inflammatory and anti-cancer drug candidate for human oral cancer treatment.

Abbreviations: ABC, avidin-biotin-peroxidase complex; ADH, alcohol dehydrogenase 1; CHX, cycloheximide; DHF, 7, 8-dihydroxyflavone; DMEM, Dulbecco's modified eagle medium; DTT, dithiothreitol; ERp44, endoplasmic reticulum resident protein 44; FBS, fetal bovine serum; HK, honokiol; IAM, idoacetamide; iNOS, inducible nitric oxide synthase; i.p., intraperitoneally; LC-MS/MS, liquid chromatography-tandem mass spectrometry; LID, ligand interaction Diagram; MMP, matrix metalloproteinases; NO, nitric oxide; OSCC, oral squamous cancer cell carcinoma; PET, positron emission tomography; PLGS, Protein lynx global server; pN, adjacent normal regions from a OSCC patient; pT, tumor regions from a OSCC patient; siERp44, ERp44 specific targeting siRNA; siRNA, small interfering RNA; TPA, 12-O-tetradecanoylphorbol 13-acetate; TUNEL, terminal deoxynucleotidyl transferase dUTP nick end labeling; XP, extra precision.

* Corresponding author. Tel.: +82 63 270 4024; fax: +82 63 270 4037.
** Corresponding author. Department of Pharmacy, College of Pharmacy, Mokpo National University, 1666 Youngsan-ro, Muan-gun, Jeonnam 534-729, Republic of Korea. Tel./fax: +82 61 450 2684.
E-mail addresses: s1004jh@gmail.com (J.-H. Shim), jichae@jbnu.ac.kr (J.-I. Chae).
[1] These authors contributed equally to this work.

http://dx.doi.org/10.1016/j.biomaterials.2015.02.091
0142-9612/

1. Introduction

Cancer is one of the most serious health problems in the developing and developed countries [1]. Advances in cancer treatment, however, continue to be limited by the identification of unique biochemical markers of malignancies. Therefore, the worldwide study of cancer chemotherapy has increased [2].

Conventional cancer treatment includes interventions such as surgery, radiotherapy and chemotherapy. However, due to the increasing rate of mortality associated with the adverse or toxic side effects of cancer chemotherapy and radiation therapy, the discovery of new anti-cancer agents derived from natural products, especially plants, is currently under investigation [3].

Honokiol (HK), a plant lignan, is a small polyphenol isolated from the bark and seed cones of the genus *Magnolia*. Recently, HK has been found to have antiangiogenic, anti-inflammatory, and anti-tumor properties in preclinical models without appreciable toxicity [4]. In a previous study, we clearly demonstrated the apoptotic effects of HK in both human oral squamous cell carcinoma (OSCC) and malignant pleural mesothelioma cell lines [5,6]. To date, a large number of natural products have been evaluated as potential chemopreventive or therapeutic phytochemicals, including HK [7]. However, there are no phytochemical agents that are effective against disseminated cancer [8]. Moreover, therapeutically relevant proteins have become attractive in modern cancer therapy, though most clinical agents have displayed a degree of polypharmacology [9].

Cancer acquires the ability to become resistant to many different types of drugs. Resistance to treatment with anti-cancer drugs results from a variety of factors including individual variations in patients and somatic cell genetic differences in tumors, even in the same tissue of origin [10]. Therefore, studies on chemotherapeutics that target specific molecules have attempted to define the mechanisms of action of phytochemicals derived from natural products. Chemical proteomics is a powerful technique combining postgenomic drug-affinity chromatography with high-end mass spectrometry analysis and bioinformatic data processing to assemble a target profile of a desired therapeutic molecule [11]. Liquid chromatography-tandem mass spectrometry (LC-MS/MS) is a powerful and widely applied method for the study of biological systems, biomarker discovery and pharmacological interventions [12]. This study was designed to investigate the anti-inflammatory anti-cancer effects of HK and its possible therapeutic target proteins in OSCC cell lines HN22 and HSC4, and tumor xenografts using the LC-MS/MS-based proteomic analysis technique.

2. Materials and methods

2.1. Materials

Dulbecco's Modified Eagle Medium (DMEM) and fetal bovine serum (FBS) were obtained from Thermo Scientific (Logan, Utah). CNBr-activated Sepharose™ 4B was obtained from GE Healthcare Biosciences (Uppsala, SE). Other reagents, unless otherwise stated, were bought from Sigma Aldrich Chemical Co. (St. Louis, MO). The following antibodies were used: anti-iNOS (C-11), anti-MMP-9 (H-129), anti-MMP-2 (H-76), anti-NFκB-p65 (F-6), anti-IκBα (FL), anti-Histone H1 (AE-4), anti-CHOP (R-20), anti-COX-2 (29), anti-Bcl-xL (A-20), anti-β-tubulin (F-1), anti-β-actin (N-21) (Santa Cruz Biotechnology, Inc., Santa Cruz, CA) and the other antibodies were from Cell Signaling (Danvers, Massachusetts).

2.2. Cell culture

Oral squamous cell carcinoma (OSCC) cell lines (HN22 and HSC4) were kindly provided from Dankook University (Cheonan, Korea) and Hokkaido University (Hokkaido, Japan), respectively. Cells were maintained in DMEM supplemented with 5% FBS and 100 U/ml each of penicillin and streptomycin, at 37 °C in a 5% CO_2 incubator.

2.3. MTS assay

The effects of HK on cell viability were estimated using MTS Assay Kit (Promega, Madison, Wisconsin). After treatment, MTS solution was added to each well for 2 h at 37 °C. The absorbance at 490 nm was recorded using a GloMax-Multi Microplate Multimode Reader (Promega, Madison, Wisconsin).

2.4. DAPI staining

The levels of nuclear condensation and fragmentation were observed by nucleic acid staining with DAPI. The fixed cells were stained with DAPI solution (2 μg/ml), and analyzed under a fluorescent microscope (Fluoview FV10i, Olympus Corporation, Tokyo, Japan).

2.5. Terminal deoxynucleotidyl transferase dUTP nick end labeling (TUNEL) assay

The apoptotic events were visualized by TUNEL assay (Roche Diagnostics GmbH, Basel, Switzerland). The stained cells were observed under a fluorescent microscope (Fluoview FV10i, Olympus Corporation, Tokyo, Japan).

2.6. Real-time PCR and RT-PCR

cDNA for RT-PCR was obtained by PCR amplification using β-actin-specific and ERp44-specific primers. Real-time PCR was performed with the SYBR green Premix Ex Taq II (Takara, Dalian, China) with Applied Biosystems StepOne Plus Real-time PCR System (Applied Biosystems, Carlsbad, CA). Primer information and PCR conditions used in the study are provided in Supplementary Table S1.

2.7. Griess assay

The amounts of NO_2^- in TPA-stimulated or normal HN22 and HSC4 cells with or without HK were determined by Griess method [13].

2.8. Zymography

Matrix metalloproteinases MMP-2 and MMP-9 activities were evaluated by gelatin zymography according to the modified Kleiner and Stetler-Stevenson method as described before [14,15].

2.9. Immunocytochemistry

To detect NFκB-p65, the cells were blocked with 1% BSA and incubated with monoclonal anti-NFκB-p65 antibody at 4 °C overnight. Probed cells were reacted with a Jackson 647-conjugated anti-mouse secondary antibody and were visualized using a fluorescent microscope (Fluoview FV10i, Olympus Corporation, Tokyo, Japan).

2.10. Isolation of mitochondria and protein fractionation

Mitochondrial and cytosolic fractions were isolated using the Mitochondria/Cytosol Fractionation Kit (Abcam) according to the manufacturer's instructions [16].

2.11. Western blot analyses

Extracted proteins samples were separated by 10% or 15% SDS-polyacrylamide gel electrophoresis and then transferred to membranes, which were incubated overnight at 4 °C with specific antibodies. The protein bands were observed after horseradish peroxidase-conjugated secondary antibody incubation, using a Pierce ECL Western Blotting Substrate (Thermo scientific, Rockford, Illinois).

2.12. Label-free quantitative analysis in either untreated or HK treated oral squamous cancer cells

The untreated or honokiol-treated cell extract was precipitated with acetone. The protein pellet was dissolved in 6 M urea buffer, reduced with 4 mM dithiothreitol (DTT) for 1 h at 37 °C, and then alkylated with 14 mM iodoacetamide (IAM) for 45 min at RT under dark condition. Excess IAM was quenched with excess DTT to provide final concentration 7 mM. Subsequently, the samples was diluted with 25 mM ammonium bicarbonate to reduce less than 1 M of urea content, and digested with trypsin (promega) at enzyme content of 2% (w/w) for 16 h at 37 °C. Trypsing reaction was terminated by formic acid ensuring final concentration of 2% (v/v). To remove urea, the tryptic peptides were cleaned up by Sep-Pak C18 cartridge (Waters). These peptides were dried by vacuum evaporation. Before LC injection, 25 mM of yeast ADH (alcohol dehydrogenase 1) peptide was spiked in each sample as internal control for normalization between independent LC-MS/MS runs. Nano LC of tryptic peptides was performed with Waters Nano LC system equipped with Water NanoEase™ Atlants™ C18, 75-μm × 25-cm reverse phase column. Binary solvent A1 and B1 contained 0.1% formic acid in water and 0.1% formic acid in acetonitrile, respectively. Total 2 μg of samples were loaded onto the column. Peptides were eluted from the column with a gradient ranging from 2 to 40% binary solvent B1 for 90 min at 0.3 μl/min. To calibrate mass accuracy, [Glu1] fibrinopeptide (m/z 785.8426) at 400 fmol/μl, was delivered from auxiliary pump of the nano LC system at 0.1 μl/min to reference sprayer of nanoLockSpray™ source. Mass spectrometry analysis of tryptic peptides was performed using Waters Synapt™ HDMS. The mass

spectrometry was operated in V-mode and positive mode nano ESI with nanospray source for all measurements. The lock mass channel for [Glu1] fibrinopeptide was sampled every 30 s. Accurate mass LC-MS/MS data were collected through alternating [low energy (MS) and elevated energy (MSE)] mode. The raw data was processed and searched in Protein Lynx Global Server (PLGS), version 2.4 (Waters). Processing of raw data was performed by following parameter: chromatographic peak width, automatic; MS TOF resolution, automatic; low energy threshold, 150 counts, elevated energy threshold, 70 counts; intensity threshold, 1500 counts. Protein identification was obtained by searching against the UniProtKB human database (release 2013_12, 20273 sequence entries) with following parameters: peptide and fragment tolerance, automatic; minimum fragment ion matches per peptide, 3; minimum fragment ion matches per protein, 7; minimum peptide matches per protein, 2; missed cleavages, 1; fixed modifications, carbamidomethyl C; variable modifications, oxidation M; false positive rate, 4. The protein list was obtained from three LC-MS/MS runs for each sample. Label-free quantitative analysis was performed with Waters IDENTITY^E expression system. The EMRT (Exact mass Retention Time) cluster table was generated by IDENTITY^E expression system. Among the EMRT cluster, only high confidence peptides were filtered and considered for quantitative analysis of differential expressed proteins between each sample. The filtering criteria to identify significant peptides and proteins was set in 2 out of 3 LC-MS/MS runs, $\geq$ 95% confidence cut off, 30% biological variation, and score value more than 80. Furthermore, at least 5 peptides were considered to calculate differential expressed protein level.

2.13. Intracellular calcium imaging

Calcium imaging was achieved by fluorescent detection of cells loaded with 4 μM Fluo-4-AM (Invitrogen) according to the manufacturer's manual. Fluo-4-AM was diluted in DMSO, and cells were loaded by diluting the dye at 4 μM with 1% BSA to improve dye solubility. Cells were immersed in the loading solution and incubated at 37 °C for 1 h. The loading solution was then washed 2–3 times with perfusion medium before fluorescence imaging. The cells were visualized using a fluorescent microscope (Fluoview FV10i, Olympus Corporation, Tokyo, Japan).

2.14. Intracellular ROS imaging

To measure ROS, we followed the procedure described by Chung et al. [17]. DCF-DA was added to cell culture media and incubated at 37 °C for 30 min. Intracellular ROS levels were visualized using a fluorescent microscope.

2.15. Mitochondrial membrane potential determinations

Changes of mitochondrial membrane potential were determined according to the manufacturer's instructions [18].

2.16. ERp44 small interfering RNA (siRNA)

On TARGET plus SMART-pool siRNA sequences targeting ERp44 and a non-targeting control were purchased from Dharmacon Research (Thermo Scientific, Lafayette, CO). Cells were transiently transfected with 50 nM siRNA using transfection reagent (Thermo Scientific, Lafayette, CO). After transfection for 72 h, the MTS assay, western blot analysis and TUNEL assay were performed to determine the effects of knocking down ERp44.

2.17. Pull-down assays

HK (1 mg) was coupled to CNBr-activated Sepharose™ 4B matrix beads (0.2 g). Cell lysates (500 μg) were incubated with HK-conjugated Sepharose 4B beads or with Sepharose 4B beads alone as control. ERp44 binding was determined by western blot analysis.

2.18. Molecular modeling for HK binding with ERp44

Computer modeling of HK with ERp44 was performed by using the Schrödinger Suite 2013 [19]. An X-RAY diffraction structure of ERp44 with a resolution of 2.6 Å (PDB ID 2R2J) [20] was obtained from the RCSB Protein Data Bank [21]. Hydrogen atoms were added consistent with a pH of 7 and all water molecules were removed, and the receptor grid for docking was generated based on site prediction by SiteMap of Schrödinger suite 2013. Then HK A-protein docking was elucidated using the program Glide by default parameters under the extra precision (XP).

2.19. Anchorage-independent cell transformation assay

Both cell lines (1.2×10^4 per well) were suspended in 1 mL BME, 10% FBS, and 0.3% agar and plated with various concentrations of HK (1, 3 and 5 μg/ml) on 3 ml of solidified BME containing 10% FBS and 0.5% agar for 30 days. Colony numbers and size were measured under a microscope.

2.20. Nude mouse xenograft

Six-week-old male BALB/c athymic (nu+/nu+) mice were purchased from Orient Bio (Kyunggi-do, Korea). The mice were maintained in accordance with the Korea Food and Drug Administration guidelines as well as the regulations for the care and use of laboratory animals of the animal ethics committee of Pohang Center for Evaluation of Biomaterials, Pohang, Gyeongbuk, Korea (POCEB-017). NH22 cells were injected subcutaneously (2.0×10^7 cells/0.1 ml PBS/animal) into the right lower flanks of mice. When the tumors had reached an average volume of 100–200 mm^3, mice were injected intraperitoneally (*i.p.*) with HK (20 and 40 mg/kg) daily for 3 weeks. The tumors were measured along the two diameter axes with calipers using the following equation; $V = p/6\{(D + d)/2\}3$, where D and d are the larger and smaller diameters, respectively. At the end of the experiment, tumors were separated from the surrounding muscle and dermis.

2.21. FDG PET imaging and quantitative imaging analysis

Positron emission tomography (PET) using fluoro-2-deoxy-D-glucose ([18F] FDG) has been shown to be an accurate technique for cancer detection, staging and monitoring of therapy in patients with various malignant cancers [22,23]. Because [18F] FDG is an analog of glucose, it is taken up by the cells *via* the glucose transporter and phosphorylated by the hexokinase, fluoro-2-deoxyglucose-6-phosphate is not processed further and remains trapped in the cells. Hence, the accumulation of [18F] FDG is an indicator of the high glucose uptake rate and hexokinase activity in tissues such as brain and brown fat.

2.22. Immunohistochemistry

Paraffin-embedded sections were deparaffinized, rehydrated, and washed in distilled water. The sections were blocked for 30 min with 3% normal horse serum diluted in PBS and incubated with anti-ERp44 antibodies. Slides were incubated with biotinylated anti-rabbit antibody and subsequently with the avidin-biotin-peroxidase complex (ABC) (Vector Laboratories, Inc., Burlingame, CA).

2.23. Tissue sample preparation

Human OSCC samples were collected from patients with their informed consent at the Chonnam National University. This study was approved by the Chonnam National University Dental Hospital Institutional Review Board (CNUDH-EXP-2014-003). The patients ranged from 51 to 82 years of age. For histochemical analysis, fresh OSCC specimens, which included both tumor tissue and adjacent normal tissue, were obtained from 15 patients between 2011 and 2012. Patients had no local recurrence, regional recurrence or metastasis after operation. Among 15 patients, three died. Two patients died of conditions unrelated to cancer recurrence or metastasis. The tissue samples were obtained from resected specimens within 30 min after surgical resection, snap frozen in liquid nitrogen, and stored at −80 °C.

2.24. Statistical analysis

Results were presented as mean ± SD of at least 3 independent experiments. Data were analyzed for statistical significance using a one-way analysis of variance. A p *value* < 0.05 was considered significant.

3. Results

3.1. Effects of HK on cell viability and apoptosis in HN22 and HSC4 cells

We confirmed HK's growth inhibitory potential in HN22 and HSC4 cells (Supplementary Fig. S1A). HN22 and HSC4 cell viability was decreased by HK in a dose- and time-dependent manner (for 24 and 48 h) (Supplementary Fig. S1B). The effect of HK on initiation of apoptosis in HN22 and HSC4 cells was determined by the TUNEL assay. HK-treated OSCC cells had increased nuclear condensation and fragmentation when compared to the control group (Supplementary Figs. S1C and D).

3.2. HK treatment reduces of MMP-2, MMP-9 and iNOS protein expression in HN22 and HSC4 cells

As a second messenger of inflammatory responses, NO is a highly reactive free radical that is involved in the activation of both MMP-2 and MMP-9. Therefore, to assess the anti-inflammatory effects of HK in TPA-stimulated HN22 and HSC4 cells, iNOS levels, NO production and MMP-2 and MMP-9 activation of were measured by western blot analysis, Griess reagent assay and gelatin zymography, respectively. As shown Fig. 1A; Supplementary Fig. S2A iNOS expression levels in HN22 and HSC4 cells were increased by TPA (20 ng/ml), but were significantly down-regulated by treatment of HK (2.5, 5, 7.5 and 10 μg/ml) in a dose-dependent

manner. Treatment of cells with HK (2.5, 5, 7.5 and 10 μg/ml) resulted in a significant down-regulation in the production of nitrite compared to controls with or without TPA (20 ng/ml) (Fig. 1B; Supplementary Fig. S2B). Moreover, consistent with diminished NO production, HK down-regulated of MMP-2 and MMP-9 activity and protein expression levels (Fig. 1C; Supplementary Fig. S2C).

3.3. Inhibitory effect of HK on NFκB activity in HN22 and HSC4 cells

Next, we investigated whether HK regulated iNOS, MMP-2 and MMP-9 expression at the genetic levels. Fig. 1D; Supplementary Fig. S2D indicated that treatment of HK (10 μg/ml) attenuated the expression of iNOS, MMP-2 and MMP-9 at the transcriptional level in both HN22 and HSC4 cells. NFκB is a transcription factor that induces the expression of genes involved in many physiological processes. Stimulation of cells with cytokines, including TPA, activates IκB kinases that phosphorylate IκBα and translocate NFκB into nucleus, which induce genes involved including inflammation, cell proliferation, and cell survival. Immunocytochemistry demonstrated that HN22 and HSC4 cells stimulated with TPA (20 ng/ml) enhanced nuclear translocation of NFκB; but HK (10 mg/ml) treatment significantly reduced the nuclear translocation of NFκB (Fig. 1E; Supplementary Fig. S2E). Western blot analysis also showed that nuc (nuclear) NFκB levels from fractionated HN22 and HSC4 cells with or without TPA (20 ng/ml) decreased by after being treatment with HK (10 μg/ml) compared to cyto (cytosolic) NFκB

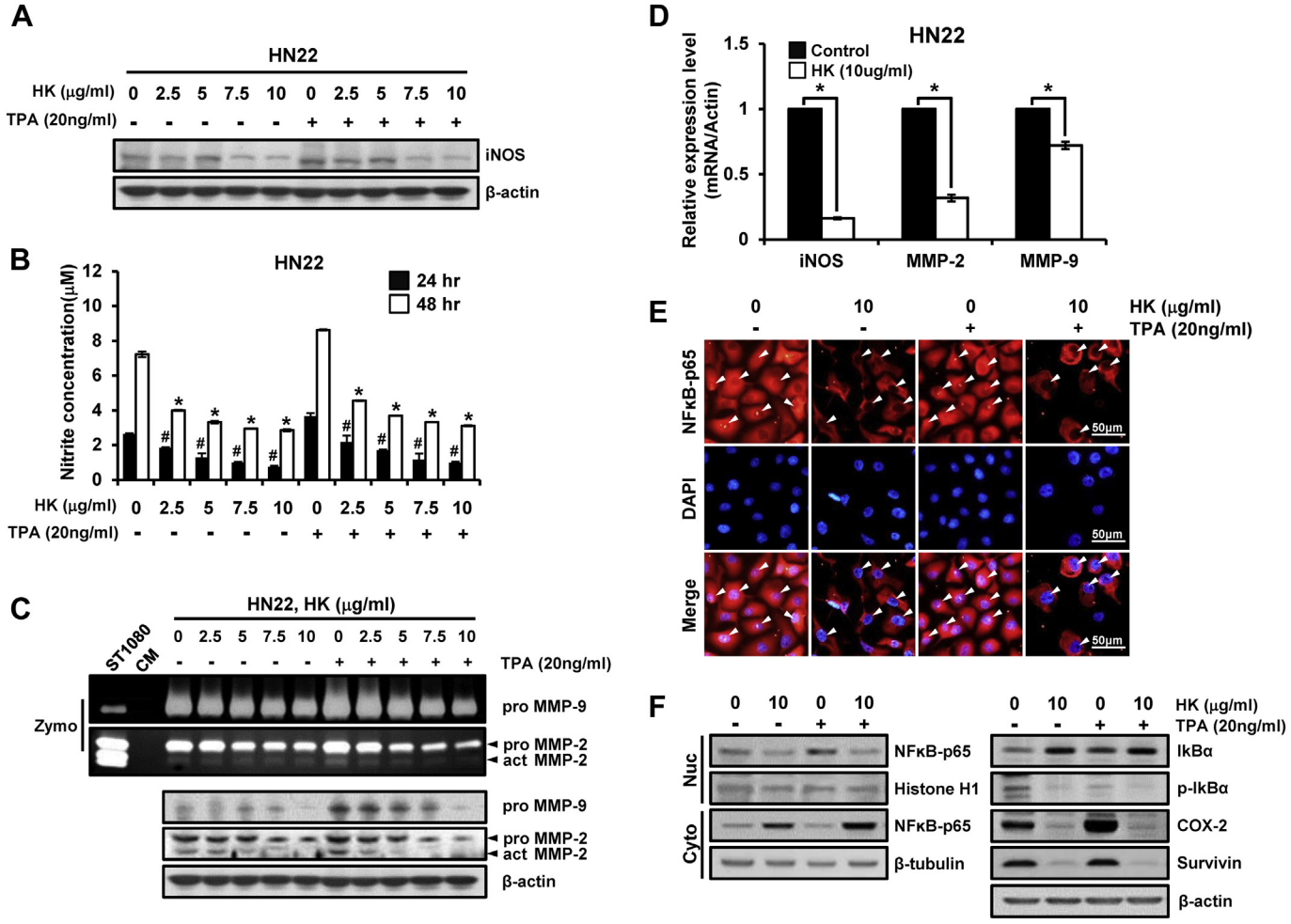

Fig. 1. A reduction of MMP-2, MMP-9 and iNOS expression by HK treatment in HN22 cells. (A) Western blots for iNOS protein in HK-treated HN22 cell with or without TPA. Expression of iNOS in HN22 cell treated with HK (2.5, 5, 7.5 and 10 μg/ml) for 48 h with or without TPA (20 ng/ml). β-actin was used as a control. Data represent mean ± SD of triplicate samples from each of 3 independent experiments. The amount of NO was determined by the Griess method as described in materials and methods. (B) Concentration of NO in HN22 cell treated with HK (2.5, 5, 7.5 and 10 μg/ml) for 24 or 48 h with or without TPA (20 ng/ml). Data represent means of 3 independent experiments; bars, SD. #, significantly different compared with untreated conditions (24 h); *, significantly different compared with untreated conditions (48 h) ($n = 3$, $p < 0.05$). (C) Representative zymographic (upper panels) and western blot (lower panels) analysis of cell culture medium and cell lysate respectively from HK (2.5, 5, 7.5 and 10 μg/ml) treated HN22 cells with or without TPA (20 ng/ml) for 24 and 48 h. Conditioned media (without TPA and HK) were used as control and HT1080 cells were used as molecular weight marker of MMP-2 and MMP-9. Three major bands are visible, corresponding to pro MMP-9, pro MMP-2 and active MMP-2. HK induced dose-dependent down-regulation of both MMP-2 and MMP-9 activities and protein expression levels. CM, conditioned media; Zymo, zymography. (D) The quantitative differences of iNOS, MMP-2 and MMP-9 at the transcriptional level were measured by real-time PCR in HN22 cells. Actin was used as a control. The levels of iNOS, MMP-2 and MMP-9 mRNA expression were significantly reduced in HK (10 μg/ml) treated HN22 cells. (E) Immunocytochemistry presented the translocation levels of NFκB into the nucleus. HN22 cells stimulated with TPA (20 ng/ml) had enhanced nuclear translocation levels of NFκB; Treatment with HK (10 μg/ml) remarkably reduced translocation of NFκB (arrowhead). (F) Western blot analysis showed that nuclear NFκB levels in fractionated HN22 cells with or without TPA (20 ng/ml) were decreased by HK treatment (10 μg/ml) compared to cytosolic NFκB levels. The expression levels of the inflammation and cell survival-related proteins, COX-2 and Survivin, respectively, were decreased. Data are presented as mean percentage levels ± SD ($n = 3$; *, $p < 0.05$). Cyto, cytosolic fraction; Nuc, nuclear fraction.

levels. Moreover, the expression levels of the inflammatory protein COX-2 and cell survival-related protetin Survivin were decreased after HK (10 mg/ml) treatment (Fig. 1F; Supplementary Fig. S2F).

3.4. Ontological classification of differentially regulated proteins in HN22 cells

Next, we performed LC-MS/MS-based proteomic analysis to elucidate the susceptible anticancer-related proteins in HN22 cells. We selected proteins that were up- and down-regulated in HK (10 μg/ml)-treated HN22 cell extracts as compared to normal HN22 cell extracts. Among the total 181 proteins identified, we confirmed 96 differentially expressed proteins from HK (10 μg/ml)-treated HN22 cell extracts compared to normal HN22 cell extracts. All of the identified proteins were clustered into 14 categories based on the biological process using information obtained from the DAVID Gene Ontology database (http://david.abcc.ncifcrf.gov) and UniProt (http://www.uniprot.org) as follows. Depending on the biological process in which the proteins were involved, they were categorized into the following groups; proteins involved in establishment of organelle localization (19.2%), cellular metabolic process (13%), cellular component assembly (12.4%), transport (10%), macromolecular complex subunit organization (10%), that regulate the stress response (6%), that regulate biological quality (5%), negative regulation of biological process (5%), response to chemical stimulus (4%), catabolic process (3%), cellular homeostasis (2%), response to biotic stimulus (2%), protein complex biogenesis (2%) and unknown proteins (7%) (Supplementary Fig. S3A). Supplementary Figs. S3B and C showed representative categories of up- and down-regulated proteins in HK (10 μg/ml) treated HN22 cell extracts. Up- and down-regulated proteins were clustered into 11 and 6 categories based on the biological process, respectively. Up-regulated proteins were categorized into groups involving response to stress (15%), response to chemical stimulus (6%), negative regulation of biological process (6%), negative regulation of cellular process (6%), regulation of biological quality (6%), regulation of molecular function (5%), cellular component assembly (5%), regulation of cellular component organization (4%), regulation of response to stimulus (4%), regulation of localization (4%) and unknown proteins (38%). Down-regulated proteins were categorized into groups involving cellular protein metabolic process (11%), cell redox homeostasis (4%), translational elongation (4%), translation (14%), protein folding (4%) and unknown proteins (7%). Next, we focused on 9 proteins that were listed in Fig. 2A; Supplementary

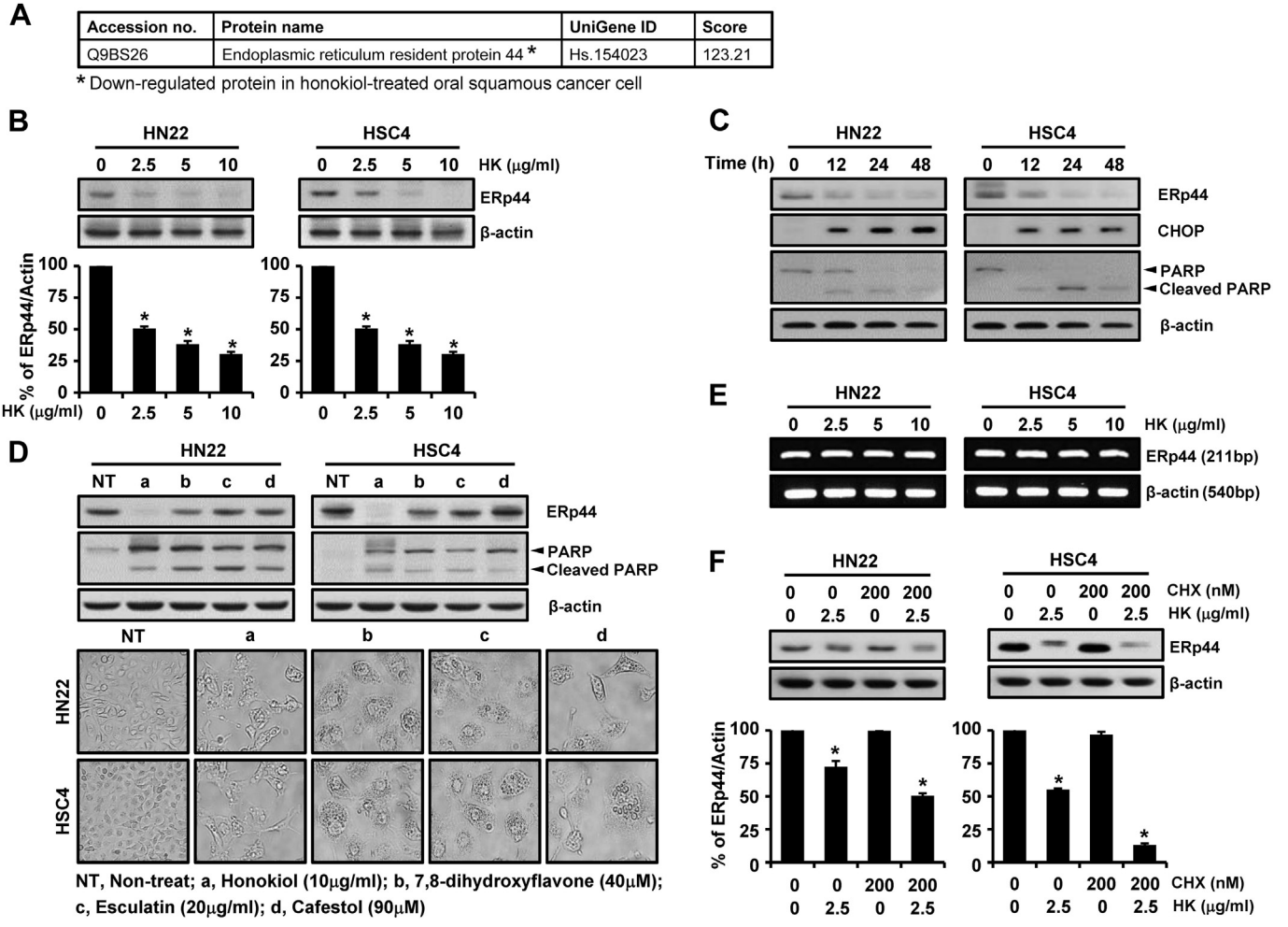

Fig. 2. The apoptotic function of ERp44 and effect of HK on ERp44 mRNA and protein expression in HN22 and HSC4 cells. (B) HK dose-dependently significantly decrease ERp44 (A) protein levels in HN22 and HSC4 cells. (C) ERp44 levels are significantly decreased and ER stress and apoptosis related proteins including CHOP and cleaved PARP were increased by HK in a time-dependent manner. (D) Apoptotic effects and expression patterns of ERp44 in HN22 and HSC4 cells treated with the various anti-cancer phytochemicals 7, 8-DHF (40 μM), esculatin (20 μg/ml) and cafestol (90 μM) treatment. PARP cleavage and morphological changes associated with apoptosis by HK (10 μg/ml), 7, 8-DHF (40 μM), esculatin (20 μg/ml) and cafestol (90 μM). Reduction of ERp44 solely by HK in both HN22 and HSC4 cells. (E and F) HK did not suppress ERp44 mRNA levels but induced ERp44 protein degradation in HN22 and HSC4 cells. Data are presented as mean percentage levels ± SD (n = 3; *, $p < 0.05$).

Table S2. Fig. 2A; Supplementary Table S2 summarized the expression changes of the up- and down-regulated proteins in HK (10 μg/ml)-treated HN22 cells, respectively and ERp44 was further analyzed by comparing their expression patterns.

3.5. The function of ERp44 on apoptosis and HK's effect on ERp44 mRNA and protein expression in HN22 and HSC4 cells

ERp44 protects against ER-stress resulting from a depletion of luminal calcium ion or a deviation from the normal oxidized redox status of the ER. ER stress-induced apoptosis was also found to be mediated *via* a target of the CHOP branch of the ER-stress response. Therefore, to determine if ERp44 expression levels were reduced by HK, HN22 and HSC4 cells were treated with various concentrations of HK (2.5, 5 and 10 μg/ml) for 48 h. As shown in Fig. 2B, treatment with HK induced a significant decrease in ERp44 protein levels in both cell lines in a dose- and time-dependent manner. In addition, ER-stress and apoptosis related proteins including CHOP and cleaved PARP, respectively, were increased by HK treatment (Fig. 2C). Remarkably, HK reduced expression levels of ERp44 specifically compared to other anti-cancer phytochemicals, as well as 7, 8-dihydroxyflavone (7, 8-DHF), esculatin and cafestol [24–26]. Fig. 2D shows the apoptotic effects and expression patterns of ERp44 in HN22 and HSC4 cells after being treated with various anti-cancer phytochemicals. PARP was cleaved and morphological changes associated with apoptosis were observed after treatment with HK (10 μg/ml), 7, 8-DHF (40 μM), esculatin (20 μg/ml) and cafestol (90 μM). ERp44 was reduced in response to HK, but not in response to 7, 8-DHF, esculatin and cafestol in both HN22 and HSC4 cells. However, HK did not suppress ERp44 mRNA in HN22 and HSC4 cells (Fig. 2E). When CHX-pretreated HN22 and HSC4 cells were incubated with HK, ERp44 protein degradation was enhanced (Fig. 2F). Collectively, these results suggested that HK-mediated degradation of ERp44 protein led to ER-stress and apoptotic cell death.

3.6. Changes in mitochondrial redox state, membrane potential and calcium precede mitochondrial dysfunction in HN22 and HSC4 cells

ER-stress leads to the release of calcium ion from the ER lumen. Mitochondrial membrane permeabilization is the critical event for the intrinsic apoptotic pathway, which results in the release of

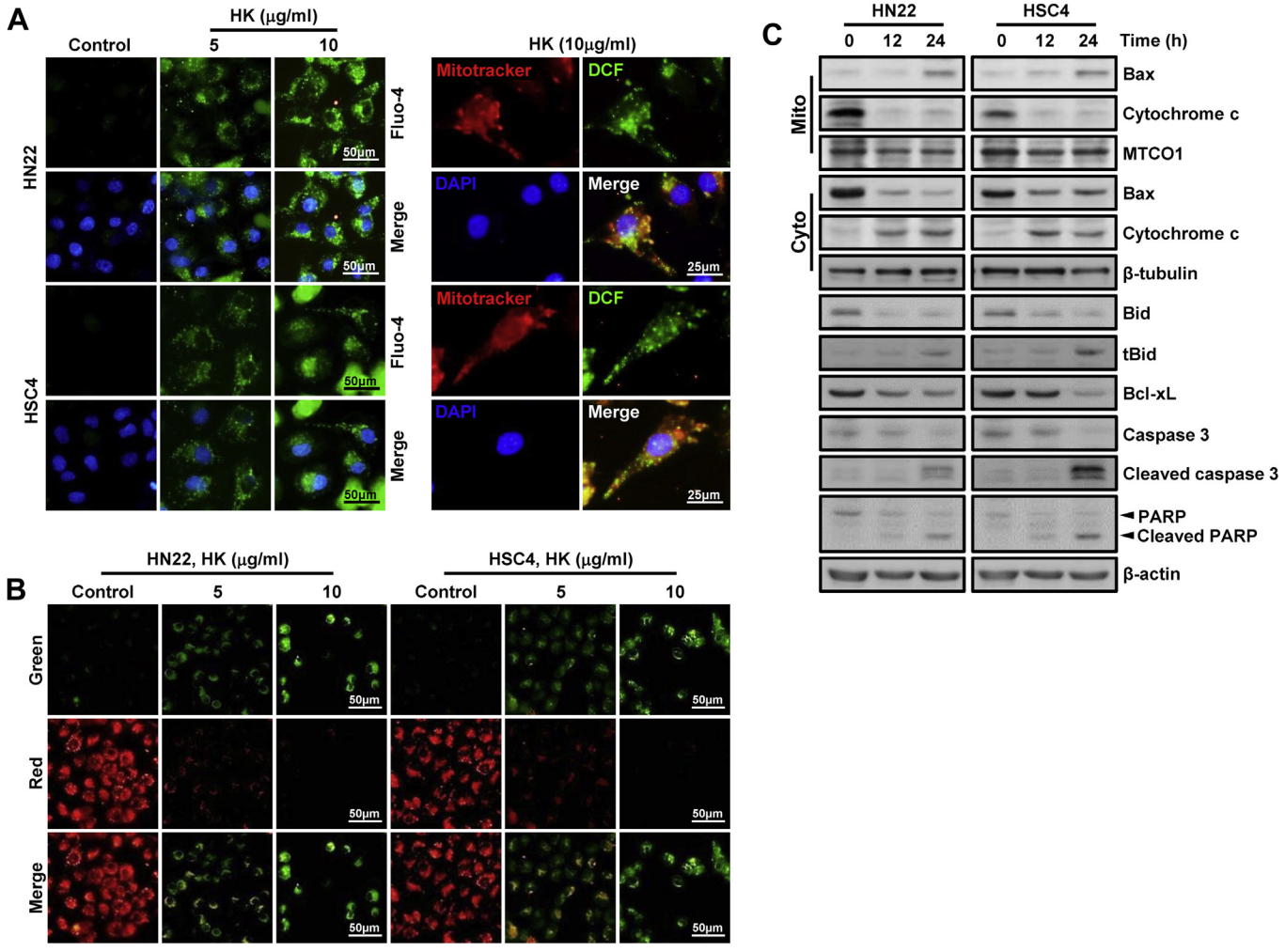

Fig. 3. Changes in the mitochondrial redox state, membrane potential and calcium precede mitochondrial dysfunction in HN22 and HSC4 cells. (A) Influence of matrix calcium ion (Fluo-4-AM), mitochondrial membrane depolarization (JC-1) and mitochondrial ROS production (DCF-DA) determined by immunofluorescence microscopy. HN22 and HSC4 cells treated with HK (5 and 10 μg/ml) for 24 h, matrix calcium ion (left panel) and mitochondrial membrane depolarization (B) increased in a dose-dependent manner. A, Mitochondrial ROS production (right panel) were followed by matrix calcium ion influx. (C) Mitochondrial apoptotic process confirmed from fractionated mitochondrial and cytosolic proteins by western blot analysis. Mitochondrial fraction was confirmed by the mitochondrial marker MTCO1 and the cytosol by β-tubulin. HK induced cytochrome *c* release and Bax expression. HK reduced Bid, Bcl-xL, Caspase 3 and PARP in a time-dependent manner. Cyto, cytosolic fraction; Mito, mitochondrial fraction.

proapoptotic factors such as Cytochrome *c* from the intermembrane and intercristae spaces. Therefore, we confirmed the functional link between ERp44 protein degradation and alterations in calcium ion and proapoptotic mitochondrial by monitoring matrix calcium ion influx in HN22 and HSC4 cells subjected to HK treatment. We loaded HN22 and HSC4 cells with Fluo-4-AM. Treatment of HN22 and HSC4 cells with HK (5 and 10 μg/ml) enhanced matrix calcium ion influx in a dose-dependent manner (Fig. 3A, left panel), which was followed by mitochondrial membrane depolarization (Fig. 3B) and mitochondrial ROS production (Fig. 3A, right panel). Anti-apoptotic members of Bcl-2 family such as Bcl-xL act primarily to preserve mitochondrial integrity by suppressing the release of Cytochrome *c*. In contrast, proapoptotic members such as Bax and Bid induce Cytochrome *c* release. Therefore, we fractionated both HN22 and HSC4 cells into mitochondrial and cytosolic proteins to determine the specific contribution of Bax, Bid and Bcl-2 family members related to the mitochondrial apoptotic process. As shown in Fig. 3C, cells treated with HK significantly induced mitochondrial Cytochrome *c* release into the cytosol followed by an increase in mitochondrial Bax. Moreover, the expression of proapoptotic proteins such as Bid, Bcl-xL, Caspase 3 were significantly decreased in a time-dependent manner.

3.7. The function of ERp44 in HN22 and HSC4 cells using siRNA technology

Next, we investigated whether ERp44 expression level had an effect on cell viability, ER-stress and mitochondrial-associated apoptosis in HN22 and HSC4 cells. We transiently transfected the ERp44 specific targeting siRNA (siERp44) into HN22 and HSC4 cells and monitored expression levels of ERp44 and cell viability at different post-transfection time points (24, 48, 72, and 96 h). ERp44 expression was suppressed for up to 72 h in both HN22 and HSC4 cells (Fig. 4A). As expected, the viability of siERp44-transfected HN22 and HSC4 cells was reduced when compared to those transfected with siCon (Fig. 4B). Results from the TUNEL assay showed that apoptosis was also significantly induced in cells where ERp44 was knocked down (Fig. 4C). Moreover, mitochondrial membrane depolarization (Fig. 4D), matrix calcium ion releasing (Fig. 4E, left panel) and mitochondrial ROS production (Fig. 4E, right

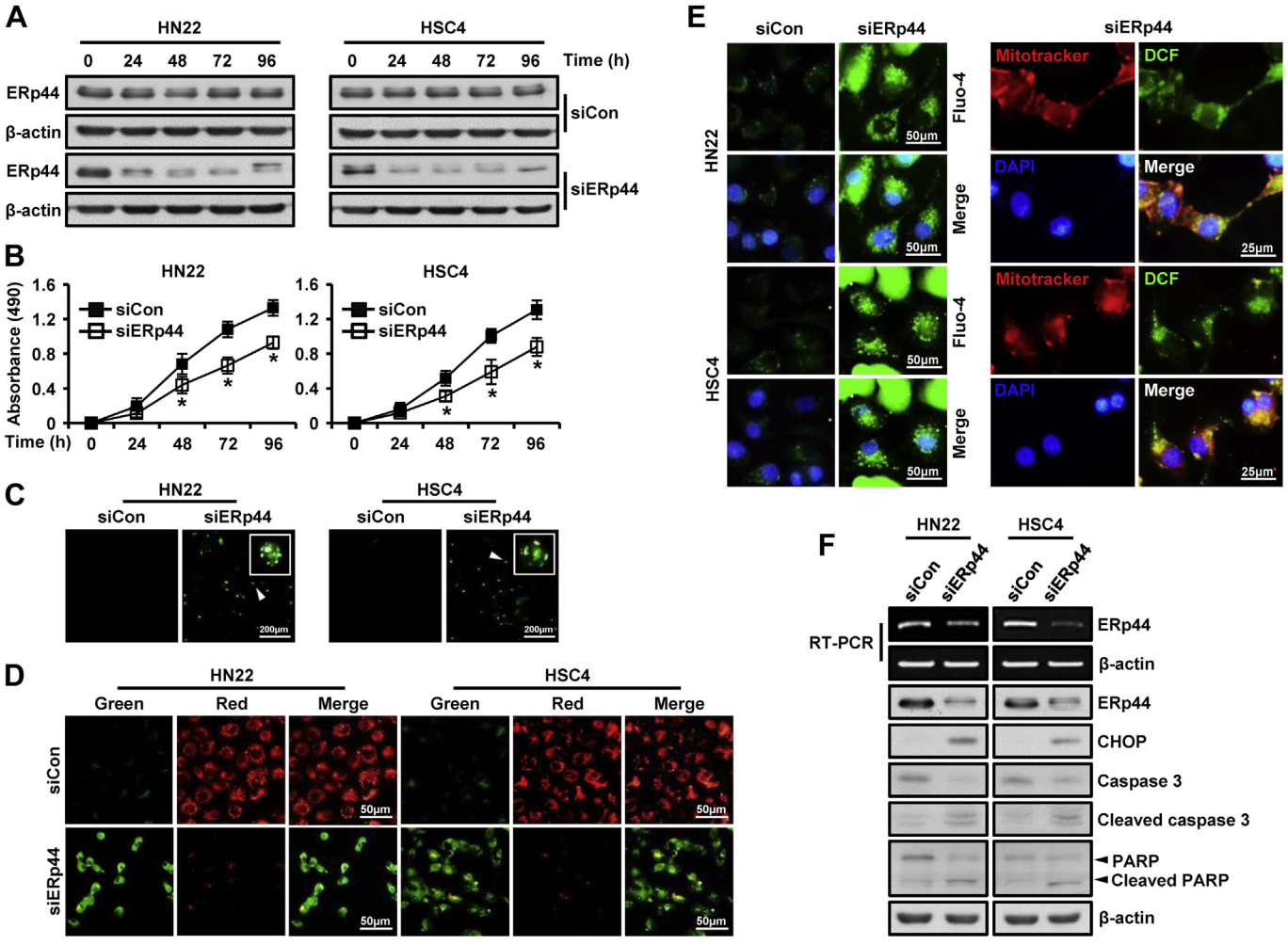

Fig. 4. The function of ERp44 in HN22 and HSC4 cells using siRNA technology. (A) ERp44 specific siERp44 or non-target siRNA, siCon, were transfected into the HN22 and HSC4 cells. (B) Cell proliferation in siCon and siERp44-transfected HN22 and HSC4 cells was quantified by an MTS assay 24, 48, 72 and 96 h post-transfection. Data are shown as the means ± SD of 3 independent experiments. The asterisk indicates a significant difference in the siERp44 transfected cells compared with the siCon transfected cells (*$p < 0.05$). Data are shown as the means ± SD of 3 independent experiments. (C) Results from the TUNEL assay indicated that apoptosis was induced in siERp44 mediated ERp44 knock-down cells. Mitochondrial membrane depolarization (D) matrix calcium ion release (E, left panel) and mitochondrial ROS production (E, right panel) were induced followed by ERp44 knock-down of HN22 and HSC4 cells. The success of the transfection of siCon or siERp44 in HN22 and HSC4 cell lysates and cDNA was determined by western blot analysis and RT-PCR, respectively. (F) The mRNA expression levels of full length Caspase 3 and PARP decreased according to the ERp44 protein, whereas cleaved Caspase 3, cleaved PARP and CHOP increased. β-actin was used as a control.

panel) were induced in ERp44 knock-down cells. The full length Caspase 3 and PARP were decreased with low ERp44 expression, whereas cleaved Caspase 3, cleaved PARP and CHOP increased expression (Fig. 4F). These results demonstrated that ERp44 expression plays an important role in the biological progression in HN22 and HSC4 cells.

3.8. HK binds with ERp44 and in silico model of HK binding with ERp44

To better understand how HK interacts with ERp44, we performed a pull-down assay. We conjugated HK to CNBr-Sepharose™ 4B beads and conducted a pull-down assay using whole cell lysates from HN22 and HSC4 cells. ERp44 directly bound to HK-Sepharose 4B beads, but not to Sepharose 4B beads alone (Supplementary Figs. S4A and B). Next, we performed the computational docking model by using the Glide docking program of Schrödinger suite 2013. In the docked models, HK binds well to ERp44 (Supplementary Fig. S4C). Supplementary Figs. S4D and E showed an enlarged view of HK binding with ERp44 and the formation of some hydrogen bonds (shown as green line) and ligand interaction Diagram (LID) for HK binding with ERp44. Some images were generated with UCSF Chimera program [27]. Supplementary Fig. S4F showed LID legend.

3.9. HK suppresses colony formation mediated through ERp44 in HN22 and HSC4 cells

We investigated whether HK affected colony formation *via* ERp44 in an anchorage-independent cell transformation assay. HK exhibited an inhibitory effect on human oral cancer cell transformation in a dose-dependent manner Fig. 5A and B). We also transiently transfected siERp44 into HN22 and HSC4 cells. Both siERp44-transfected HN22 and HSC4 cells significantly inhibited colony formation (Fig. 5C and D).

3.10. The anti-tumor effect of ERp44 in nude mouse xenograft models

A tumor xenograft model of HN22 in nude mice was used to investigate the *in vivo* anti-tumor activities of HK. Two to four weeks after the inoculation of HN22 cells, tumor diameter reached up to 20 mm and whole-body imaging was performed by PET/CT. PET/CT images of animals bearing HN22 cancer cells were acquired 30 min post-injection of [18F] FDG *via* the tail vein (100uCi). The images were reconstructed with a 2-dimensional ordered-subsets expectation maximum algorithm. [18F] FDG uptake was significantly reduced in HK-treated tumors compared to control tumors (Fig. 6A). Moreover, HK significantly reduced tumor growth without body weight changes (Fig. 6B and C). We also compared both ERp44 and iNOS expression in tumor tissue from control and HK-treated mice by immunohistochemistry and H&E staining. High levels of ERp44 and iNOS were observed in the control tumors, but expression levels were decreased in tumors from HK-treated mice (Fig. 6D). Histologic analysis revealed induction of apoptosis in tumors derived from mice treated with HK than in controls. *In situ* TUNEL staining was carried out for tissue sections of tumors (Fig. 6E). HK treatment caused a significant percentage of TUNEL-positive apoptotic cells ($p < 0.05$). While ERp44 expression was significantly reduced in HK-treated tumor tissue, levels of cleaved PARP and CHOP were increased compared to control tumor tissue (Fig. 6F). Finally,

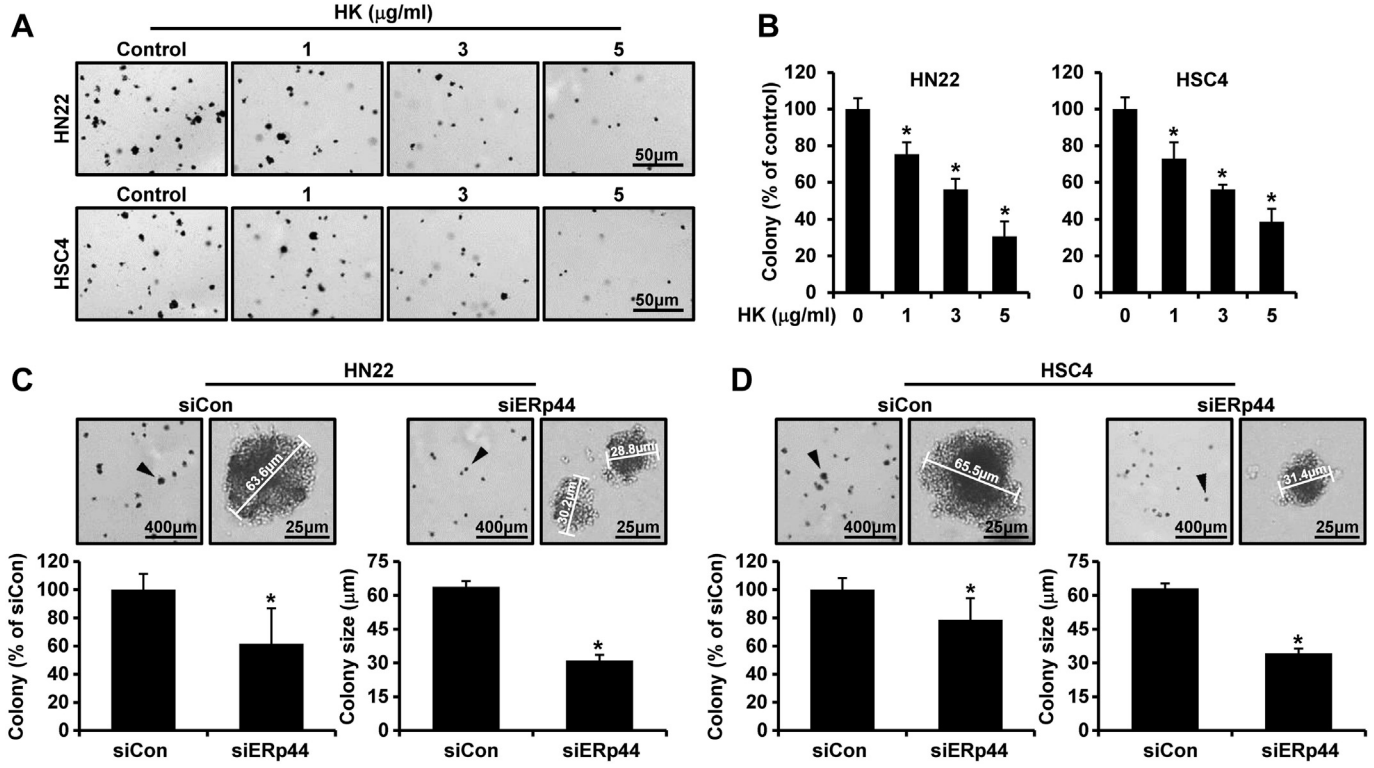

Fig. 5. HK inhibited colony formation mediated through ERp44 in OSCC cell lines HN22 and HSC4. (A and B) HN22 and HSC4 cells were treated with HK (1, 3 and 5 μg/ml) in 1 ml of 0.3% basal medium Eagle's agar containing 10% FBS in the anchorage-independent cell transformation assay. Both cells were incubated at 37 °C in a 5% CO_2 incubator for 30 days and colonies were counted. The counted colonies were expressed as mean ± SD (n = 3; *, $p < 0.05$) *vs.* control cells. (C and D) Both HN22 and HSC4 cells were transfected with siCon or siERp44, and an anchorage-independent cell transformation assay was carried out as described in materials and methods. Colony numbers and size were measured as described above and results are expressed as mean ± SD (n = 3; *, $p < 0.05$) for triplicate experiments.

both ERp44 and iNOS expression were investigated in oral squamous cell carcinoma (pOSCC) samples taken from patients. Elevated levels of brown (ERp44) and immunofluorescence staining (iNOS) were observed in pT tissues compared with pN tissues (Fig. 6G). These results indicated that both ERp44 and iNOS were overexpressed in oral cancer. HK could exert a strong anti-tumor effect on the OSCC model, acting as a potent apoptosis-inducing agent *in vivo*.

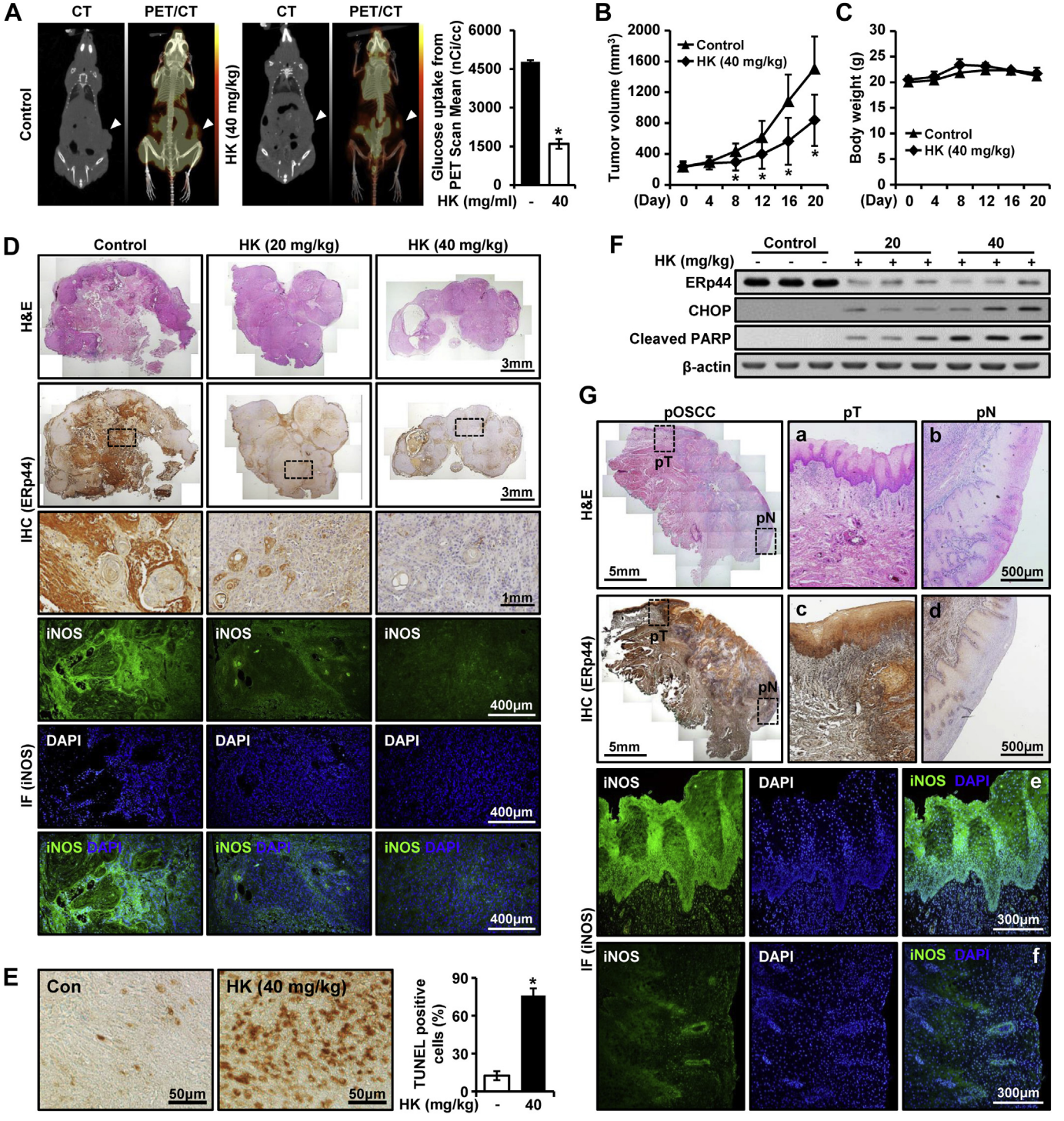

Fig. 6. The anti-tumor effect of ERp44 in nude mouse xenograft models. BALB/c nude mice bearing HN22 cell were treated with DMSO (control) or HK (20, 40 mg/kg) for 21 days. (A) PET/CT images and glucose uptake. PET/CT image demonstrating an area of FDG accumulation (arrowhead). (B and C) Tumor volume and body weight were determined as described in Methods. Data represent mean of 10 animals; bars show SD. $^*p < 0.05$. (D) H&E staining and histological analysis of ERp44 and iNOS levels in tumors from control and HK-treated mice. (E) Apoptosis was detected in tumor tissues by the TUNEL assay as described in materials and methods. Columns, mean of 3 animals; bars, SD. $^*p < 0.05$ indicates statistically significant differences from the untreated group. (F) HK reduced ERp44 expression in tumor tissue and increased cleaved PARP and CHOP as compared to untreated tumor tissue. (G) pOSCC tissues were immunostained with antibodies against ERp44 and iNOS. pOSCC tissues were deparaffinized and immunostained using anti-ERp44 and anti-iNOS antibodies. Strong expression of ERp44 and iNOS were observed in the pT compared with the pN. Enlarged view of the pT and pN indicated by H&E and immunohistochemical staining. pT, tumor regions from a OSCC patient (a, c and e); pN, adjacent normal regions from a OSCC patient (b, d and f).

4. Discussion

Cancer is one of the leading causes of death worldwide [28]. Current chemotherapeutic agents have serious side effects in patients. Therefore, the developments of anti-cancer drug have focused on cytostatic or cytotoxic compounds that cause tumor regression. These paradigms have been expanded to include the pre-selection of molecular targets as part of in the discovery of therapeutic agents. An important element of preclinical and clinical screening of target-oriented drugs is their effectiveness on the specific molecular targets. Therefore, the discovery and development of anti-cancer agents necessitate changes in the anti-cancer drug preclinical and clinical screening paradigms [29].

HK is a bioactive natural product and well-known for its anti-inflammatory, anti-angiogenic, antioxidative and anti-cancer properties *in vitro* and in preclinical models [28]. Although some progress has been made, the cellular targets of HK remains unknown. Therefore, to identify the multifunctional molecular targets of HK, further investigation was conducted at the proteomic level. Proteomic analysis of HK treated-HN22 cells was performed to obtain differential protein expression patterns using a LC-MS/MS-based approach. Bioinformatics analysis subclassified proteins involved in the anti-inflammatory and anti-cancer effects of HK.

The molecular messenger NO is one of the smallest signaling molecules that are associated with inflammation and cancer. NO is synthesized by 3 isoforms of the enzyme NO synthase, of which iNOS is particularly involved in tumorigenesis [30]. In our results, HK not only inhibited cell growth, but also induced apoptosis in OSCC cell lines (Supplementary Fig. S1). Moreover, iNOS expressions at the protein and mRNA levels were reduced by HK treatment (Fig. 1A and B; Supplementary Figs. S2A and B). NO is an important regulator of various MMPs, which are overexpressed in metastatic cancers and promote cancer cell migration [31]. In our studies, MMP-2 and MMP-9 activities were substantially reduced by HK treatment (Fig. 1C and D; Supplementary Figs. S2C and D). Additionally, NFκB nuclear translocation was reduced by HK treatment (Fig. 1E; Supplementary Fig. S2E). We also confirmed that COX-2 and Survivin, the inflammation- and survival-related proteins, respectively, were down-regulated by HK treatment (Fig. 1F; Supplementary Fig. S2F).

Next, LC-MS/MS-based analysis was done to elucidate the susceptible anticancer-mediated proteins in OSCC cells. Among the identified total 181 proteins, 96 proteins were differentially expressed in HK-treated HN22 cell extracts. The identified total proteins were clustered into 14 (Supplementary Fig. S3A) categories; up- and down-regulated proteins were clustered into 11 (Supplementary Fig. S3B) and 6 (Supplementary Fig. S3C) categories based on their roles in various biological processes. Out of 96 proteins, biological functions of 9 proteins were listed in Fig. 2A; Supplementary Table S2.

HK significantly reduced ERp44 expression levels, while the induction of ER-stress-induced transcription factor and CHOP were observed in OSCC cells (Fig. 2B). ERp44 acts as an anchoring protein for ER-resident proteins that lack an ER retention signal and in many instances, a family of ER oxidoreductases including ERp44 catalyzes oxidative protein folding [32].

We demonstrated that HK treatment led to reduction of NO levels with the unexpected induction of CHOP in OSCC cells (Fig. 2C). We therefore hypothesized that the induction of the ER stress-induced transcription factor by HK is not regulated by NO but by other mediators, such as ERp44. Notably, HK specifically reduced the expression of ERp44 as compared to other anti-cancer phytochemicals, as well as 7, 8-DHF, esculatin and cafestol (Fig. 2D). While ERp44 protein was degraded in response to HK treatment, ERp44 mRNA expression was not affected (Fig. 2E and F). After ERp44 degradation, ER calcium ion flows into the cytoplasm (Fig. 3A, left panel). ERp44 is a key regulator of protein secretion, calcium signaling and redox regulation [33] *via* interaction with IP_3R1 in a calcium ion, redox and pH dependent manner [34].

In pathologic conditions, excessive influx of cytosolic calcium ion into the mitochondria triggers dysfunction of the mitochondrial membrane permeabilization [35] with mitochondrial ROS induction In our studies, we confirmed that mitochondrial membrane depolarization and mitochondrial ROS production (Fig. 3A, right panel and 3B) were followed by an influx of matrix calcium ion after HK treatment. Moreover, HK induced a significant release of cytochrome *c* from the mitochondria, followed by an increase in mitochondrial Bax and a significant decrease in the expression levels of the proapoptotic proteins Bid, Bcl-xL, Caspase 3 and PARP (Fig. 3C). Similarly, mechanisms of ER stress and apoptotic responses were significantly induced by siERp44 mediated ERp44 knock-down in OSCC cells (Fig. 4).

Remarkably, HK bound directly to ERp44 (Supplementary Figs. S4A and B) and hydrogen bonds were formed between HK and ERp44 (Supplementary Figs. S4C–F). Additionally, we investigated whether HK affected colony formation through ERp44. The anchorage-independent cell transformation assay showed an inhibitory effect due to HK treatment (Fig. 5A and B). ERp44 was identified as a key factor for carcinogenesis in this model (Fig. 5C and D). Finally, we demonstrated high levels of ERp44 and iNOS expression in pOSCC, and also presented preclinical evidence of HK's potent anti-tumor activity using tumor xenografts of OSCC and HN22 cells. HK significantly inhibited tumor growth both *in vivo* and *in vitro* experiments (Fig. 6).

5. Conclusion

In summary, HK inhibited inflammation and induced apoptosis by suppressing both iNOS/NO and ERp44 expression in HN22 and HSC4 cells and xenograft tumors. Based on these results, HK appears to be a potent anti-inflammatory and anti-cancer drug candidate for human oral cancer treatment.

Acknowledgments

This research was supported by the National Research Foundation Stem Cell Program (NRF-2014M3A9B4043056), Republic of Korea.

Appendix A. Supplementary data

Supplementary data related to this article can be found online at http://dx.doi.org/10.1016/j.biomaterials.2015.02.091.

References

[1] Murray SA, Grant E, Grant A, Kendall M. Dying from cancer in developed and developing countries: lessons from two qualitative interview studies of patients and their carers. BMJ 2003;326:368.
[2] Hoekstra R, Verweij J, Eskens FA. Clinical trial design for target specific anticancer agents. Investig New drugs 2003;21:243–50.
[3] Cragg GM, Newman DJ. Plants as a source of anti-cancer agents. J Ethnopharmacol 2005;100:72–9.
[4] Fried LE, Arbiser JL. Honokiol, a multifunctional antiangiogenic and antitumor agent. Antioxidants Redox Signal 2009;11:1139–48.
[5] Chae JI, Jeon YJ, Shim JH. Downregulation of Sp1 is involved in honokiol-induced cell cycle arrest and apoptosis in human malignant pleural mesothelioma cells. Oncol Rep 2013;29:2318–24.
[6] Kim DW, Ko SM, Jeon YJ, Noh YW, Choi NJ, Cho SD, et al. Anti-proliferative effect of honokiol in oral squamous cancer through the regulation of specificity protein 1. Int J Oncol 2013;43:1103–10.
[7] Akao Y, Nakagawa Y, Iinuma M, Nozawa Y. Anti-cancer effects of xanthones from pericarps of mangosteen. Int J Mol Sci 2008;9:355–70.

[8] Gottesman MM. Mechanisms of cancer drug resistance. Annu Rev Med 2002;53:615–27.
[9] Chamrad I, Rix U, Stukalov A, Gridling M, Parapatics K, Muller AC, et al. A miniaturized chemical proteomic approach for target profiling of clinical kinase inhibitors in tumor biopsies. J Proteome Res 2013;12:4005–17.
[10] Krol M, Pawlowski KM, Majchrzak K, Szyszko K, Motyl T. Why chemotherapy can fail? Pol J veterinary Sci 2010;13:399–406.
[11] Tate EW. Recent advances in chemical proteomics: exploring the post-translational proteome. J Chem Biol 2008;1:17–26.
[12] Jankevics A, Merlo ME, de Vries M, Vonk RJ, Takano E, Breitling R. Separating the wheat from the chaff: a prioritisation pipeline for the analysis of metabolomics datasets. Metabolomics: Off J Metabolomic Soc 2012;8:29–36.
[13] Barker SL, Clark HA, Swallen SF, Kopelman R, Tsang AW, Swanson JA. Ratiometric and fluorescence-lifetime-based biosensors incorporating cytochrome c' and the detection of extra- and intracellular macrophage nitric oxide. Anal Chem 1999;71:1767–72.
[14] Hajighasemi F. Profiles of MMP-2 expression in Jurkat, Molt-4 and U937 cells. Iranian J Immunol: IJI 2011;8:120–6.
[15] Yodkeeree S, Chaiwangyen W, Garbisa S, Limtrakul P. Curcumin, demethoxycurcumin and bisdemethoxycurcumin differentially inhibit cancer cell invasion through the down-regulation of MMPs and uPA. J Nutr Biochem 2009;20:87–95.
[16] Zhang Q, Pan J, North PE, Yang S, Lubet RA, Wang Y, et al. Aerosolized 3-bromopyruvate inhibits lung tumorigenesis without causing liver toxicity. Cancer Prev Res 2012;5:717–25.
[17] Chung YM, Lee SB, Kim HJ, Park SH, Kim JJ, Chung JS, et al. Replicative senescence induced by Romo1-derived reactive oxygen species. J Biol Chem 2008;283:33763–71.
[18] Kuo JJ, Chang HH, Tsai TH, Lee TY. Curcumin ameliorates mitochondrial dysfunction associated with inhibition of gluconeogenesis in free fatty acid-mediated hepatic lipoapoptosis. Int J Mol Med 2012;30:643–9.
[19] UniProt C. Reorganizing the protein space at the Universal Protein Resource (UniProt). Nucleic Acids Res 2012;40:D71–5.
[20] Wang L, Wang L, Vavassori S, Li S, Ke H, Anelli T, et al. Crystal structure of human ERp44 shows a dynamic functional modulation by its carboxy-terminal tail. EMBO Rep 2008;9:642–7.
[21] Berman HM, Westbrook J, Feng Z, Gilliland G, Bhat TN, Weissig H, et al. The protein data bank. Nucleic Acids Res 2000;28:235–42.
[22] Reske SN, Kotzerke J. FDG-PET for clinical use. Results of the 3rd German Interdisciplinary Consensus Conference, "Onko-PET III", 21 July and 19 September 2000. Eur J Nucl Med 2001;(28):1707–23.
[23] Younes-Mhenni S, Janier MF, Cinotti L, Antoine JC, Tronc F, Cottin V, et al. FDG-PET improves tumour detection in patients with paraneoplastic neurological syndromes. Brain: J Neurol 2004;127:2331–8.
[24] Lee KA, Chae JI, Shim JH. Natural diterpenes from coffee, cafestol and kahweol induce apoptosis through regulation of specificity protein 1 expression in human malignant pleural mesothelioma. J Biomed Sci 2012;19:60.
[25] Lee SY, Lim TG, Chen H, Jung SK, Lee HJ, Lee MH, et al. Esculetin suppresses proliferation of human colon cancer cells by directly targeting beta-catenin. Cancer Prev Res 2013;6:1356–64.
[26] Park HY, Kim GY, Hyun JW, Kim ND, Kim CG, Kim WJ, et al. 7,8-dihydroxyflavone induces G1 arrest of the cell cycle in U937 human monocytic leukemia cells via induction of the Cdk inhibitor p27 and down-regulation of pRB phosphorylation. Oncol Rep 2012;28:353–7.
[27] Pettersen EF, Goddard TD, Huang CC, Couch GS, Greenblatt DM, Meng EC, et al. UCSF Chimera–a visualization system for exploratory research and analysis. J Comput Chem 2004;25:1605–12.
[28] Arora S, Singh S, Piazza GA, Contreras CM, Panyam J, Singh AP. Honokiol: a novel natural agent for cancer prevention and therapy. Curr Mol Med 2012;12:1244–52.
[29] Chabner BA, Roberts Jr TG. Timeline: chemotherapy and the war on cancer. Nat Rev Cancer 2005;5:65–72.
[30] Crowell JA, Steele VE, Sigman CC, Fay JR. Is inducible nitric oxide synthase a target for chemoprevention? Mol cancer Ther 2003;2:815–23.
[31] Choi BD, Jeong SJ, Wang G, Park JJ, Lim DS, Kim BH, et al. Secretory leukocyte protease inhibitor is associated with MMP-2 and MMP-9 to promote migration and invasion in SNU638 gastric cancer cells. Int J Mol Med 2011;28:527–34.
[32] Malhotra JD, Kaufman RJ. Endoplasmic reticulum stress and oxidative stress: a vicious cycle or a double-edged sword? Antioxidants Redox Signal 2007;9:2277–93.
[33] Cortini M, Sitia R. From antibodies to adiponectin: role of ERp44 in sizing and timing protein secretion. Diabetes Obes Metab 2010;12(Suppl. 2):39–47.
[34] Higo T, Hattori M, Nakamura T, Natsume T, Michikawa T, Mikoshiba K. Subtype-specific and ER lumenal environment-dependent regulation of inositol 1,4,5-trisphosphate receptor type 1 by ERp44. Cell. 2005;120:85–98.
[35] Armstrong JS. Mitochondrial membrane permeabilization: the sine qua non for cell death. BioEssays: News Rev Mol Cell Dev Biol 2006;28:253–60.